Genes & Diseases

RESEARCH WATCH

Targeting UDP-α-D-glucose 6-dehydrogenase alters the CNS tumor immune microenvironment and inhibits glioblastoma growth

Daqian Zhan [a,b,1], Fatih Yalcin [c,d,1], Ding Ma [a,e], Yi Fu [a],
Shuang Wei [f], Bachchu Lal [a], Yunqing Li [a], Omar Dzaye [c,g],
John Laterra [a,h], Mingyao Ying [a], Hernando Lopez-Bertoni [a,**],
Shuli Xia [a,*]

[a] Neurology, Hugo W. Moser Research Institute at Kennedy Krieger, Johns Hopkins University School of Medicine, Baltimore, MD 21205, USA
[b] Department of Critical Care Medicine, Tongji Hospital, Huazhong University of Science and Technology, Wuhan, Hubei 430074, PR China
[c] Department of Radiology and Neuroradiology, Charité, Berlin 10117, Germany
[d] Russell H. Morgan Department of Radiology and Radiological Science, Johns Hopkins University School of Medicine, Baltimore, MD 21205, USA
[e] Department of Respiratory and Critical Care Medicine, Tongji Hospital, Huazhong University of Science and Technology, Wuhan, Hubei 430074, PR China
[f] University Hospital Center Schleswig Holstein, Department of Neurosurgery, Kiel, Schleswig-Holstein 24105, Germany
[g] Departments of Neurology, Oncology and Neuroscience, Johns Hopkins University School of Medicine, Baltimore, MD 21205, USA
[h] Blood and Cell Therapy Institute, University of Science and Technology of China, Anhui Provincial Hospital, Hefei, Anhui 230026, PR China

* Corresponding author. Hugo W. Moser Research Institute at Kennedy Krieger, Department of Neurology, Johns Hopkins School of Medicine, 707 N. Broadway, Room 400K, Baltimore, MD 21205, USA. Fax: +443 923 2695.
** Corresponding author. Hugo W. Moser Research Institute at Kennedy Krieger, Department of Neurology, Johns Hopkins School of Medicine, 707 N. Broadway, Room 400C, Baltimore, MD 21205, USA. Fax: +443 923 2695.
E-mail addresses: LopezBertoni@kennedykrieger.org (H. Lopez-Bertoni), xia@kennedykrieger.org (S. Xia).
Peer review under responsibility of Chongqing Medical University.
[1] Co-first authors.

Abstract   Glioblastoma (GBM, WHO grade IV glioma) is the most common and lethal malignant brain tumor in adults with a dismal prognosis. The extracellular matrix (ECM) supports GBM progression by promoting tumor cell proliferation, migration, and immune escape. Uridine diphosphate (UDP)-glucose 6-dehydrogenase (UGDH) is the rate-limiting enzyme that catalyzes the biosynthesis of glycosaminoglycans that are the principal component of the CNS ECM. We investigated how targeting UGDH in GBM influences the GBM immune microenvironment, including tumor-associated microglia/macrophages (TAMs) and T cells. TAMs are the main immune effector cells in GBM and can directly target tumor cells if properly activated. In co-cultures of GBM cells and human primary macrophages, UGDH knockdown in GBM cells promoted macrophage phagocytosis and M1-like polarization. In orthotropic human GBM xenografts and syngeneic mouse glioma models, targeting UGDH decreased ECM deposition, increased TAM phagocytosis marker expression, reduced M2-like TAMs and inhibited tumor growth. UGDH knockdown in GBM cells also promoted cytotoxic T cell infiltration and activation in orthotopic syngeneic mouse glioma models. The potent and in-human-use small molecule GAG synthesis inhibitor 4-methylumbelliferone (4-MU) was found to inhibit GBM cell proliferation and migration *in vitro*, mimic the macrophage and T-cell responses to UGDH knockdown *in vitro* and *in vivo* and inhibit growth of orthotopic murine GBM. Our study shows that UGDH supports GBM growth through multiple mechanisms and supports the development of ECM-based therapeutic strategies to simultaneously target tumor cells and their microenvironment.

Introduction

Glioblastoma (GBM, grade IV glioma) is the most common and lethal malignant brain tumor in adults with extensive tumor cell proliferation and invasion.[1] The tumor microenvironment, including the extracellular matrix (ECM), tumor-associated microglia/macrophages (TAMs) and T cells, contributes to the malignant features of GBM and its resistance to immune-surveillance and immunotherapeutics. Recent advances in T cell-based therapeutics including CAR-T and immune checkpoint blockade (e.g., PD-1/PD-L1) highlight the promise of cancer immunotherapy. However, patients across multiple cancers, especially GBM, have not shown robust responses to these approaches.[2] Increasing the objective response rate to T cell-based immunotherapy remains a pressing challenge. On the other hand, TAMs, which comprise 30%–40% of a GBM mass, predominantly exhibit an immunosuppressive M2-like phenotype that support tumor growth.[3] Strategies that switch TAMs towards their M1-like immune stimulatory phenotype are highly desired.

The ECM is a physiologically active component of living tissues that constantly undergoes dynamic remolding to influence cell adhesion, migration, proliferation, and cell-cell communication.[4] The deposition and remodeling of ECM components are tightly regulated; dysregulated ECM leads to impaired cell behaviors and a consequent break down of tissue homeostasis, contributing to many pathological conditions, including cancer. Dysregulated ECM drives tumor progression by promoting tumor cell proliferation/migration, cancer stem cell maintenance, and immune evasion.[5] The ECM influences communication between tumor cells and immune cells in the tumor microenvironment as ECM molecules bind to their cognate receptors, including integrin, CD44, and pattern recognizing receptor (PPR) to influence immune cell function.[6] In addition, the ECM functions as a depot for growth factors, cytokines, and chemokines, thereby influencing autocrine/paracrine signaling that modulates function of tumor-associated immune cells. The ECM has been reported to inhibit T cell proliferation and activation[7] and dense ECM forms a physical barrier to prevent T cell infiltration into tumors.[8] Thus, therapeutic strategies that target oncogenic ECM are promising approaches to inhibiting multiple oncogenic mechanisms by simultaneously target tumor cells and their tumor promoting microenvironment.

The ECM in the brain is unique in composition and organization as it contains relatively small amounts of fibrous proteins (e.g., collagen, fibronectin) but high amounts of glycosaminoglycans (GAGs), including hyaluronic acid (HA) and proteoglycans (CSPG, HSPG, etc.).[9] GAGs are long, unbranched poly-saccharides with repetitive units of disaccharide, one of which is UDP-glucuronic acid (UDP-GlcUA). Uridine diphosphate (UDP)-glucose 6-dehydrogenase (UGDH) is the rate-limiting enzyme for synthesizing UDP-GlcUA,[10–12] and high levels of UGDH correspond to poor survival in a subset of GBM patients.[13] While abnormal ECM is a distinctive characteristic of glial tumors, the impact of UGDH on GBM malignancy has not been explored until our recent publication[13] showing the multi-faceted functions of UGDH that drive GBM malignancy. In patient-derived GBM neurosphere cells enriched for cancer stem cells, UGDH knockdown (KD) decreased ECM components and inhibited GBM cell proliferation/

migration *in vitro* and *in vivo*. The impact of targeting UGDH on the tumor immune microenvironment, including TAMs and T cells, is largely unknown.

Several small molecules, including 4-methylumbelliferone (4-MU), have been shown to inhibit UGDH, but none of them are specific.[14] 4-MU is a coumarin derivative that phenocopies the effect of UGDH KD by depleting UDP-GlcUA, thereby potently inhibiting GAG synthesis, especially HA. 4-MU has also been shown to downregulate UGDH[15] and hyaluronan synthases.[16] Due to its low toxicity, 4-MU is used as a dietary supplement, has been approved in Asia and Europe for human use, and is currently under clinical testing in the USA (NCT00225537, NCT02780752). The clinical experience to date suggests 4-MU is a safe and well-tolerated drug. 4-MU has efficacy against prostate, ovarian and breast cancers in preclinical models.[17] The effect of 4-MU on CNS malignancies or the tumor immune microenvironment is relatively unknown.

Since the ECM plays an important role in immune response, we asked how genetic and pharmacological targeting of ECM synthesis alters the tumor cell–immune cell interactions. We found that UGDH knockdown in GBM cells or 4-MU treatment promotes an immune stimulatory tumor microenvironment by affecting both TAMs and T cells. Our findings show that disrupting oncogenic ECM though UGDH inhibition has a high potential to simultaneously target GBM tumor cells and the tumor immune microenvironment within the CNS.

Materials and methods

Reagents and cell cultures

All reagents were purchased from Sigma–Aldrich (St Louis, MO) unless otherwise stated. The GBM patient-derived neurosphere line HSR-GBM1A (GBM1A) was originally derived from Dr. Vescovi's group.[18] GFP$^+$ control and UGDH knock down (KD) GBM1A cells were generated with GFP tagged UGDH shRNA as we described in Oyinlade et al.[13] Mouse glioma cell line GL261 was original purchased from American Type Culture Collection (ATCC, Manassas, VA). All cell lines are free from mycoplasma and authenticated with short tandem repeat profiling by Johns Hopkins Genetic Resources Core facility using Promega Gene Print 10 system (Madison, WI). GBM1A neurosphere cells were cultured in Dulbecco's modified Eagle's medium (DMEM)/F12 medium (Thermo Fisher Scientific, Waltham, MA) supplemented with epidermal growth factor (EGF) (Peprotech, Rocky Hill, NJ) and fibroblast growth factor (FGF) (Peprotech). GL261 cells were cultured in Dulbecco's Minimum Essential Media (Thermo Fisher Scientific) supplemented with 10% fetal calf serum (FCS, Gemini Bio-products, West Sacramento, CA). All cells were grown at 37 °C in a humidified incubator with 5% CO_2, and passaged every 2–4 days.

Viral transfection

To knock down UGDH expression in mouse glioma GL261 cells, we used two TRC shRNA lentiviral vectors (pLKO.1-puro vector) purchased from Johns Hopkins chemCORE Facility.[13] HEK 293FT cells were co-transfected with control non-silencing shRNA or mouse UGDH shRNA

vectors and packaging plasmids using Lipofectamine 3000 following the manufacturer's protocol. GL261 cells were infected with viral particles supplemented with 10 μg/ml polybrene and selected with puromycin (2 μg/ml). UGDH knockdown GL261 cells were maintained in media containing 2 μg/ml of puromycin for further experiments.

Cell proliferation analysis

For cell proliferation analysis, $0.5–1 \times 10^5$ cells were seeded in triplicates in 6-well plates. After 24 hours (h) of incubation, the cells were treated with 4-MU (0.5 mM and 1.0 mM) and/or high molecular weight HA (HMW-HA, 100 μg/ml). At each indicated time point, the cells were trypsinized and manually counted using a hemocytometer. The number of cells, based on the average count of the three wells, was compared among the different groups from three independent experiments.

Serial dilution assay for neurosphere formation

Neurosphere formation assays were performed with limited cell dilutions at 5, 10, 20, 50, 100 cells in 96-well plates in neurosphere medium as we reported previously.[19] After 10–14 days of culture, sphere-positive wells were scored by observation under an inverted microscope. Neurosphere-forming frequency was analyzed by ELDA (Extreme Limiting Dilution Analysis), an online data analysis program at http://bioinf.wehi.edu.au/software/elda/index.html.[20]

Cell migration

Cell migration assays were performed using transwell chambers as we previously described.[21] GBM1A cells (1×10^5) were placed into the upper wells of transwells containing neurosphere medium without EGF/FGF. Neurosphere cell culture medium containing EGF/FGF was added to the lower chamber. After 24 h, cells that migrated through the filter were fixed with Diff-Quick kit (Thermo Fisher Scientific) and stained with 4′,6-diamidino-2-phenylindole (DAPI). Cell migration was quantified by counting cells on five randomly selected fields per transwell in at least three independent experiments.

Human primary macrophage cultures and co-cultures

Human whole blood from healthy donors was obtained from a local hospital in Leukopak. Peripheral blood mononuclear cells (PBMCs) were isolated using Ficoll–Paque PLUS (GE Healthcare, Chicago, IL).[22,23] PBMC derived monocyte was isolated using a Human Pan Monocyte Isolation Kit (Miltenyi Biotec, Gaithersburg, MD) according to the manufacturer's protocol. Monocytes were then re-suspended in RPMI medium 1640 supplemented with 10% fetal bovine serum. GM-CSF or M-CSF (PeproTech) was added to the culture medium at the concentration of 20 ng/ml to differentiate monocyte into M0 macrophages. One week later, cells were ready to use for co-culture studies.

Phagocytosis analysis was performed as we previously described.[24] Briefly, human primary macrophages were

seeded into 12 well plates (1.5 × 10^5/well). Cancer cells were labeled with Carboxyfluorescein succinimidyl ester (CFSE, eBioscience, San Diego, CA) following the manufacture's protocol. CFSE labeled target cells (3 × 10^5) were added to macrophages and incubated at 37 °C for 2 h. Macrophages were then stained CD11c-APC (Thermo Fisher Scientific) for 30 min. Phagocytosis was assessed by flow cytometry and evaluated by the percentage of dual-labeled cells (CFSE$^+$/CD11c-APC$^+$) over total APC$^+$ cells. Flow-cytometry data were acquired using a BD Beckman cytometer. All data were further analyzed by FlowJo software.

For macrophage polarization studies, PBMC-derived M0 macrophages were cultured in 6-well plates at 3 × 10^5 cells per well. GBM cells were added to macrophages (1:1) for 24 h. The two cell populations were separated by trypsin as macrophages adhered much stronger to culture surfaces. Total RNA was extracted from macrophages and subjected to further studies.

Quantitative real-time PCR (qRT-PCR)

Total RNA was extracted using RNeasy Mini Kit (Qiagen, Mansfield, MA). After reverse transcription using cDNA reverse transcriptase (Applied Biosystems, Carlsbad, CA) and Oligo (dT) primer, qRT-PCR was performed using SYBR Green PCR Mix (Applied Biosystems) and IQ5 detection system (Bio-Rad, Hercules, CA). Primer sequences used in this study were listed in Table S1. Relative gene expression was normalized to GAPDH.

Immunoblotting

Total cellular protein was extracted with radio-immunoprecipitation assay (RIPA) buffer containing protease and phosphatase inhibitors as we reported previously.[25] Protein concentration was determined by the Coomassie Protein Assay (Thermo Fisher Scientific) according to the manufacturer's recommendations. SDS-PAGE was performed with 30 μg total proteins using 4%–12% gradient Tris-glycine gels (Thermo Fisher Scientific). Primary antibodies used for this study include anti-UGDH (Cell signaling Technology, Danvers, MA) and β-actin. Proteins were detected and quantified using the Odyssey Infrared Imager (LI-COR Biosciences, Lincoln, NE) with secondary antibodies labeled by IRDye infrared dyes (LI-COR Biosciences) and normalized to β-actin.

Immunofluorescence and immunohistochemistry staining

Immunofluorescence staining was performed on Cryostat tumor sections according to the procedure we previously described.[21] The primary antibodies used for immunofluorescent staining are the following: Iba-1 (Wako, Ginza); CD107a (Thermo Fisher Scientific); iNOS (Thermo Fisher Scientific); TMEM119 (Abcam, Cambridge); Arginase-1 (Cell signaling Technology); TGM2 (Cell signaling Technology); Ki67 (Bethyl Laboratories, Montgomery, TX); granzyme B (Cell Signaling); FoxP3 (Cell Signaling). For HA staining, HA-binding protein (b-HABP) was used. Immunofluorescence images were taken under a fluorescent microscope and analyzed using Axiovision software (Carl Zeiss, Germany). Positive staining was quantified by Image J or manually counted.

Immunohistochemistry studies were performed as we described in Lal et al.[26] Briefly, PFA-fixed brain sections were incubated with citrate-based antigen unmasking buffer (Vector Laboratories, Burlingame, CA) at 90 °C for 30 min. Endogenous peroxidase was inactivated by 3% hydrogen peroxide for 5 min. Sections were incubated with blocking buffer (5% goat serum) at room temperature for 1 h, followed by primary antibodies at 4 °C overnight. After washing, sections were incubated with biotinylated secondary antibody at room temperature for 1 h. For signal detection, after washing, sections were incubated with buffer containing streptavidin-HRP followed by DAB (Vector Laboratories). Sections were counterstained with 0.5% methyl green. Primary antibodies used for IHC studies were: anti-CD4 (Cell Signaling) and anti-CD8 (Cell Signaling).

T cell proliferation, activation, and migration

Human T cells were isolated from PBMCs using a pan-T cell selection kit from Miltenyi, then labeled with CFSE at 1.5 μg/ml for 15 min at room temperature. Staining was quenched by adding 5 folds cold complete culture medium, incubated on 4 °C for 5 min. Cells were counted after washing and treated with CD3/CD28 T cell activation beads (Miltenyi) and recombinant human IL-2 (10 ng/ml) follow instructions from Miltenyi. Activated T cells were added to tumor cells at a final effector-to-target cell ratio of 0.5:1, 1:1, and 2:1 in RPMI 1640 plus 10% FBS for 3 days. T cell proliferation was measured using flow cytometry analysis of histograms of CFSE. T cell activation will be measured by flow cytometry analysis of CD69-APC (Biolegend, San Diego, CA).

T cell transmigration assays were tested using transwells with a pore size of 3 μm (Corning, Corning, NY). Briefly, control or UGDH KD GBM1A cells were placed into the upper chambers of transwells (0.5 × 10^5/well) and grew for 4 days to become confluent; human T cells (1 × 10^6) were activated by CD28/CD3 antibody + IL2 (10 ng/ml) for 24 h as we described above. Activated T cells were placed into transwells containing confluent GBM cells; after 18 h, transmigrated T cells in the medium of lower chambers (10% FCS) were collected and quantified.

Glioma formation in animal models

All animal protocols were approved by the Johns Hopkins School of Medicine Animal Care and Use Committee. For intracranial xenografts, 10,000 viable GBM1A neurosphere cells in 2 μL of PBS were injected into the right caudate/putamen of severely immunodeficient mice (SCID, 8-week-old female) by stereotactic injection. For mouse glioma models, 8-week-old female immunocompetent C57BL/6 mice received 10,000 viable GL261 cells. Mice were sacrificed after different time points by perfusion, and the brains were fixed with 4% paraformaldehyde for 48 h followed by 30% sucrose for 72 h. Frozen brains were embedded with Tissue-Tek O.C.T. Compound (VWR, Radnor, PA) and cut at 20 μm. Tissue sections were also processed for standard hematoxylin and eosin (H&E) staining.

Tumor volumes were quantified by measuring cross-sectional tumor areas on H&E-stained cryostat sections using computer-assisted image analysis as previously described. Tumor volumes were estimated based on the formula: Vol = (sq. root of maximum cross-sectional area).

4-MU treatment

4-MU was pressed into the mouse chow at 5% (wt/wt) by TestDiet (Richmond, VA) and irradiated before shipment, as previously described.[27] This dose was previously calculated to deliver approximately 150−250 mg/mouse/day.[28] Mice were initiated on the 4-MU chow between six and eight weeks of age and were maintained on this diet until they were euthanized, unless otherwise noted.

Statistical analysis

Data were analyzed using Prizm software (GraphPad). All results reported here represent at least three independent replications. Post hoc tests included the Students t-test and the Tukey multiple comparison tests as appropriate. Data are represented as mean value $\pm$ standard error of the mean (SEM), and significance was set at $P < 0.05$.

Results

UGDH KD GBM cells activated human primary macrophages in co-cultures

We used several co-culture systems to investigate how UGDH KD in GBM cells affects tumor cell-immune cell interactions.[13] Monocytes isolated from human peripheral blood mononuclear cells (PBMCs) were differentiated into M0 macrophages as described in Materials and Methods.[22,23] To determine if UGDH-KD increases the phagocytic capacity of macrophages, we co-cultured control shRNA transduced cells (Con) and UGDH KD GBM1A cells (both are GFP^+, FL1) with macrophages (labeled with APC-CD11c, FL4), followed by flow cytometry analysis.[24] Compared with control GBM1A cells, the phagocytosis index (GFP^+/APC^+ vs. APC^+) increased $\sim$2-fold in macrophages co-cultured with UGDH KD GBM cells (Fig. 1A, B; $P < 0.05$). Co-cultures were stained for CD107a, a lysosome-associated membrane protein associated with phagolysosome formation,[29] and Iba1, a specific marker for macrophages. When compared to the effect of control GBM cells, the UGDH KD cells increased macrophage CD107a staining intensity with a punctuated staining pattern (Fig. 1C), further supporting increased phagocytosis in response to UGDH expression inhibition.

In addition to phagocytosis capacity, we investigated how UGDH KD affects macrophage polarization. Monocytes differentiated into M0 macrophages using either GM-CSF or M-CSF responded similarly to LPS or IL4 stimulus (Fig. S1A, B). Control and UGDH KD GBM cells were co-cultured with GM-CSF or M-CSF-differentiated macrophages (1:1) for 24 h and then separated using trypsin as macrophages adhere much stronger to culture surfaces. qRT-PCR revealed that UGDH KD GBM cells increased macrophage expression of M1 markers CD40/CD80/IL12B/TNFA without altering expression of M2 markers CD163/CD206/IL10/TGFB (Fig. 1D, E, and Fig. S1C, $P < 0.05$). These results show that inhibiting UGDH in GBM cells promotes neighboring macrophages to express an M1-like immune stimulatory phenotype.

UGDH KD in GBM cells alters TAM morphology and increases phagocytosis in vivo

We previously showed that UGDH knockdown decreases GBM cell GAG synthesis in vitro and in vivo,[13] now we asked how if decreased ECM components alter interactions between tumor cells and TAMs in vivo. Immunodeficient (SCID) mice were implanted with 10,000 viable control or UGDH KD GBM cells in the caudate-putamen and sacrificed at post-implantation days 7 and 56 ($n = 5$) to evaluate TAM phenotypes during GBM growth. The TAM morphology and marker expression at PID 7 were quite similar in control and UGDH KD tumors. Specifically, dense $Iba1^+$ TAMs were found at the injection sites of both control and UGDH KD GBM1A cells. Compared with resting microglia in non-injected hemispheres that displayed long thin processes (Fig. S2), most TAMs at the tumor implantation sites displayed typical an amoeboid morphology void of processes (Fig. 2A, B, left panels). In comparison to the weak CD107a expression of the resting microglia (Fig. S2), TAMs in both control and UGDH KD tumors expressed elevated cytoplasmic CD107a (Fig. 2A, B, middle panels). High magnification revealed many small cytoplasmic compartments showing high intensity CD107a staining (Fig. 2A, B, enlarged in right panels). Differences in TAM morphology and marker expression were observed between control and UGDH KD GBMs at PID 56, when control animals were pre-morbid due to large tumors while UGDH KD tumors were still small as we previously reported.[13] Specifically, in control tumors, $Iba1^+$ TAMs showed weak CD107a staining with a perinuclear pattern (Fig. 2C). In contrast, $Iba1^+$ TAMs in UGDH KD GBM showed enlarged and round cell bodies and intense CD107a staining throughout the cytoplasm (Fig. 2D). These findings show that UGDH KD induces TAMs to maintain a phagocytic and likely anti-tumor phenotype after prolonged tumor growth.

UGDH KD alters immune cell infiltration and inhibits growth of murine GBM in vivo

We used murine GL261 glioma cells that form intracranial tumors in syngeneic immunocompetent C57BL/6 mice with both the innate and adaptive immune systems to build on our findings in SCID mice. UGDH expression was inhibited using two distinct mouse UGDH shRNAs, which achieved more than 60% reduction of UGDH protein (Fig. 3A). There was no difference in the proliferation of control non-silencing (NS) and UGDH KD GL261 cells in vitro (Fig. 3B). However, UGDH KD significantly decreased intracranial tumor growth in syngeneic mice, with an average tumor volume of 38 mm^3 vs. 20 mm^3 at post-implantation week 3 in control and UGDH KD groups, respectively (Fig. 3C, D, S3A, $P < 0.05$, $n = 8$ from two independent experiments). Tumor staining with UGDH Ab confirmed decreased UGDH in tumors derived from UGDH KD GL261 glioma cells (Fig. 3E, F, S3B). On the other hand, Ki67 staining did not show a
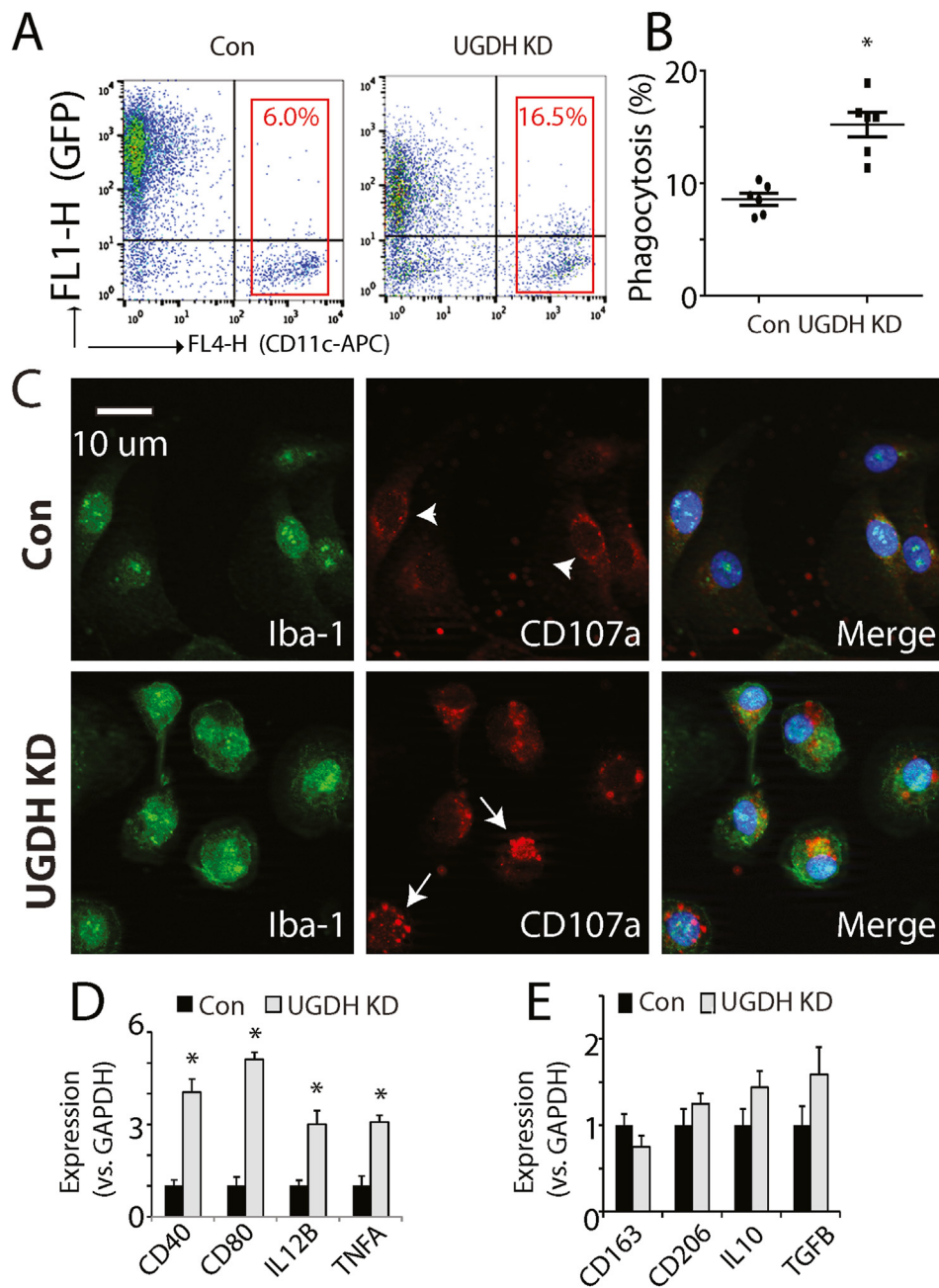
Figure 1 UGDH KD GBM cells activated macrophages. **(A,B)** GBM cells were labeled with CFSE (FL1) and incubated with macrophages for 2 h (2:1), followed by staining with APC-conjugated anti-human CD11b antibody (FL4). Phagocytosis index was defined as % of CFSS$^+$APC$^+$ cells *vs.* all APC$^+$ cells. UGDH KD increased phagocytosis of macrophages. **(C)** Immunofluorescence (IF) staining of Iba1 and CD107a in macrophages from co-cultures (2 h). **(D,E)** qRT-PCR of M1 and M2 polarization markers in macrophages co-cultured with non-silencing control cells (Con) and UGDH KD GBM1A cells (1:1) for 24 h. Data represent Mean ± SEM. $n = 6$. *: $P < 0.05$; ***: $P < 0.001$.

significant difference in the proliferation rate of control and UGDH KD glioma cells *in vivo* (Fig. 3G, H, and Fig. S3C), suggesting that the tumor microenvironment was involved in the decreased tumor growth in UGDH KD gliomas.

The morphology, density, and activation of TAMs in control and UGDH KD GL261 gliomas were examined using antibodies against Iba1 and CD107a. Immunofluorescence (IF) staining revealed that the morphology of TAMs in control and UGDH KD mouse gliomas did not differ, and there was a slight but non-significant increase in the density of Iba1$^+$ cells (*vs.* DAPI$^+$) in UGDH KD gliomas (42–49%) compared with control tumors (40%) (Fig. 3I, J, and Fig. S3D). Consistent with our findings in SCID mice, there was a ∼25–30% increase in the intensity of phagocytosis marker CD107a in TAMs within the UGDH KD tumors (Fig. 3K, $P < 0.05$). The association between UGDH KD, elevated
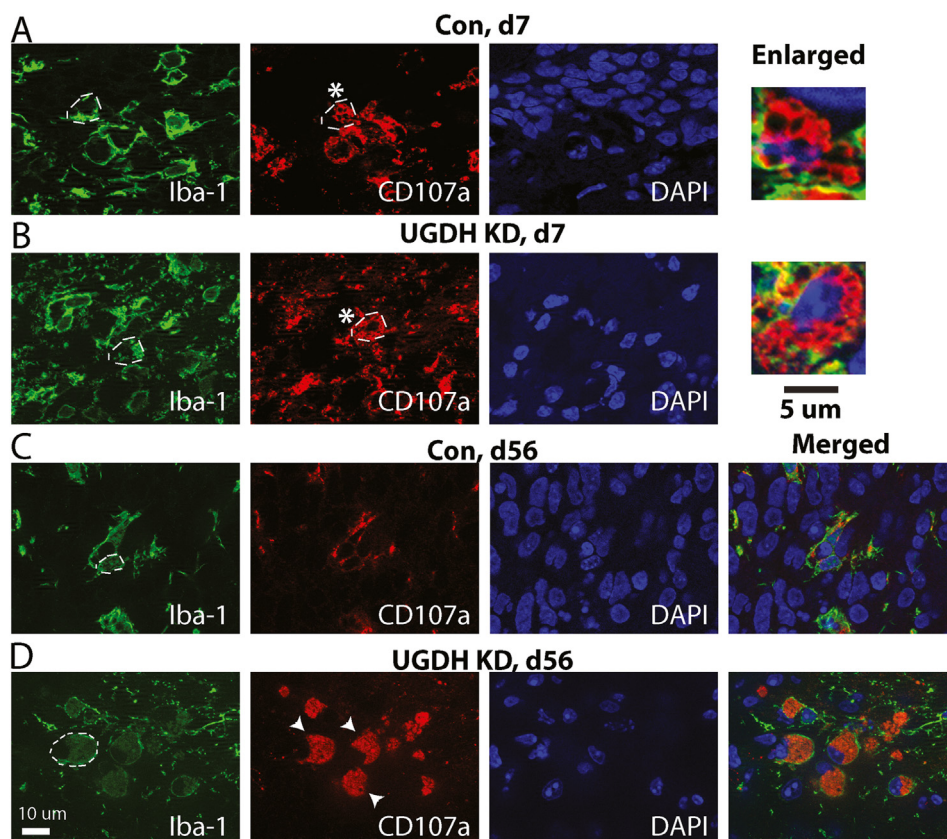
Figure 2 UGDH KD GBM cells promoted CD107a expression in TAMs *in vivo*. **(A,B)** Iba1 and CD107a staining in control and UGDH KD brain tumors 7 days after implantation of human GBM1A neurosphere cells. TAMs in both tumors showed amoeboid morphology and elevated CD107a staining intensity. **(C,D)** Iba1 and CD107a staining in tumors 56 days after tumor cell implantation. Compared with control tumors (C), TAMs in UGDH KD tumors showed a hypertrophic morphology with elevated CD107a staining (arrowheads in D).

CD107a expression and tumor growth inhibition suggests induction of anti-tumor TAM activity by UGDH KD in the immune-competent GL261 model.

We further examined the polarization of TAMs in control and UGDH KD gliomas using IF staining of commonly used markers, including iNOS (for M1-like phenotype) and Arg-1 (for M2-like phenotype). Little or no iNOS expression was detected in TAMs from control and experimental tumors (data not shown). On the other hand, both control and UGDH KD gliomas recruited Arg1$^+$ TAMs, and the density of Arg1$^+$ cells (*vs*. DAPI) was decreased from ~23% to 17.3% by UGDH KD (Fig. 3L, M, S3E, $P < 0.05$). Our results suggest that UGDH KD recruited fewer M2 TAMs in gliomas.

Taking advantage of the syngeneic mouse glioma model, we further investigated how UGDH knockdown affects T cell infiltration and activation in syngeneic glioma models. IHC/ IF staining revealed that compared with control tumors, there was an ~80% increase in CD8$^+$ cytotoxic T cells (Fig. 4A, B, S3F, $P < 0.05$), ~2 fold increase in CD4$^+$ T helper cells (Fig. 4C, D, S3G, $P < 0.05$), and a decrease in Fox3P$^+$ regulatory T cells (Tregs) in UGDH KD tumors

(Fig. 4E, F, S3H, $P < 0.05$). Furthermore, we examined CD8$^+$ T cell activation using granzyme B (GZMB) IF staining and found a ~3 fold increase in GZMB$^+$ cells in UGDH KD tumors (Fig. 4G, H, S3I, $P < 0.05$). Our results suggest that UGDH KD in glioma cells increased T cell infiltration and activation. Taken together, we found that targeting UGDH in GBM cells significantly increased the anti-tumor function of both innate and adaptive immune cells *in vivo*.

UGDH KD in GBM cells promoted human T cell migration, proliferation, and activation *in vitro*

To validate that the observed tumor cell−T cell interactions in mouse glioma models can be recapitulated in human tumor cell−T cell interactions, we established several co-cultures containing human glioma cells and human T cells isolated from PBMCs using a pan-T cell selection kit. We first asked if UGDH KD GBM cells increased T cell migration using transwells with a pore size of 3 μm. Control or UGDH KD GBM cells were placed into the upper chambers of transwells (0.5×10^5/well) and grown for 4 days until confluent.
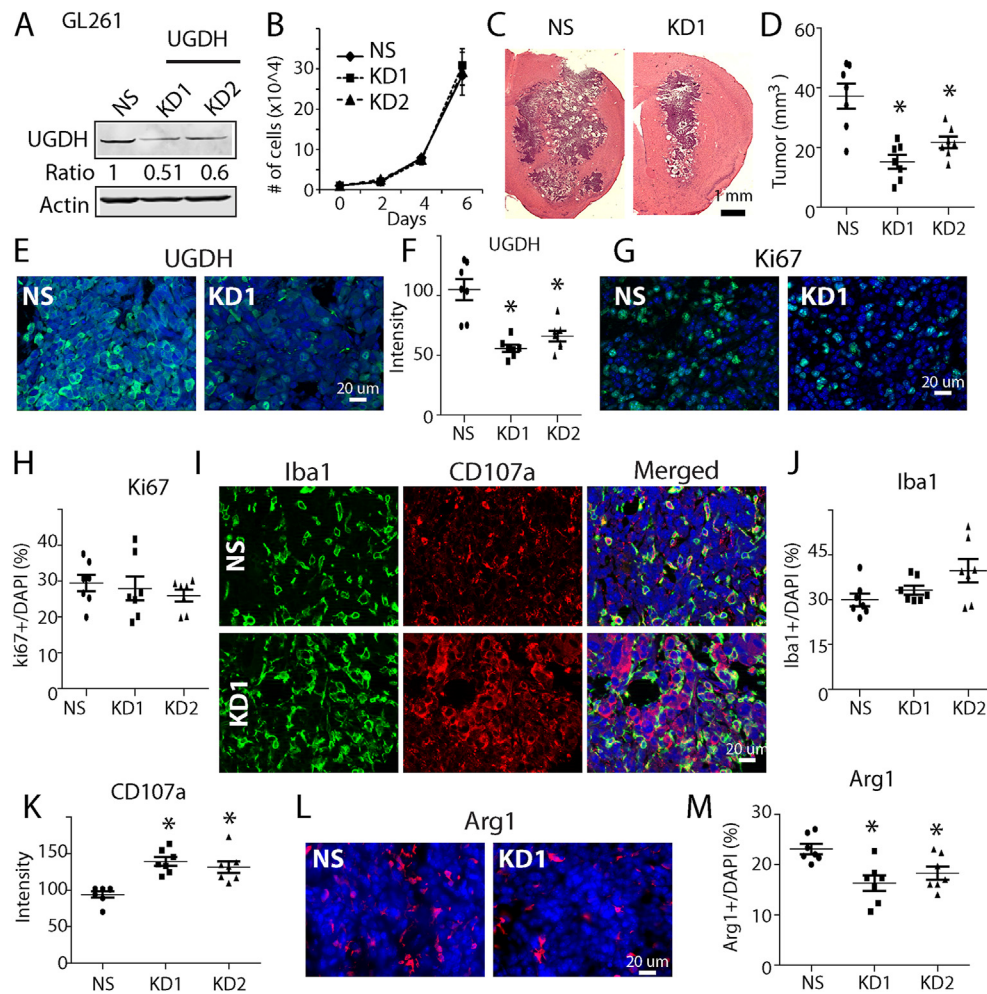
Figure 3 UGDH KD in mouse glioma models inhibited GBM growth. **(A)** Immunoblotting confirmed that compared to non-silencing cells (NS), UGDH knockdown by two distinct UGDH shRNAs in mouse GL261 glioma cells. **(B)** Cell growth of control NS and UGDH KD GL261 cells *in vitro*. **(C,D)** H&E staining and quantification of control and UGDH KD gliomas 3 weeks after tumor implantation. **(E,F)** IF staining of UGDH in gliomas confirmed decreased UGDH expression in UGDH KD gliomas. **(G,H)** Ki67 staining and quantification of control and UGDH KD gliomas. **(I,K)** IF staining and quantification of Iba1 and CD107a in control and UGDH KD mouse gliomas at week 3. **(L,M)** IF staining and quantification of Arg1 mouse gliomas. Data represent Mean ± SEM. *: $P < 0.05$.

T cells (1×10^6) activated by CD28/CD3 Ab + IL2, as we described in Materials and Methods, were placed into the transwells containing confluent GBM cells (Fig. 4I). Eighteen hours later, T cells that migrated into the lower chamber medium (10% FCS) were collected and quantified. UGDH KD GBM cells induced T cell migration 4-fold compared to control cells (Fig. 4I, $P < 0.05$).

To investigate how UGDH KD GBM cells affect T cell proliferation and activation *in vitro*, we co-cultured GBM cells with activated and CFSE-labeled T cells (1:1). After three days, T cell proliferation was measured based on the histogram of CFSE signal using flow cytometry, and T cell activation was based on the expression of marker CD69.[30] An example of cell gating and CFSE/CD69 signals from co-cultures was shown in Figure S4. Compared with control co-cultures, UGDH KD GBM cells significantly increased T cell proliferation by ~30% (Fig. 4J, $P < 0.05$). T cell

activation marker CD69 was significantly increased by ~80% when co-cultures with UGDH GBM cells (Fig. 4K, $P < 0.05$). Collectively, our *in vitro* results suggested that inhibiting ECM synthesis in human GBM cells increased human T cell migration, proliferation, and activation, consistent with our *in vivo* findings in mouse glioma models.

The GAG synthesis inhibitor 4-MU alters GBM cell—macrophage interactions and inhibits GBM cell growth

We employed 4-methylumbelliferone (4-MU, hymecromone), a small molecule inhibitor of UDP-GlcUA synthesis and GAG synthesis, to examine the translational relevance of our findings from genetically modified tumor cell models. 4-MU decreased UGDH expression by more than 40% in both GBM1A
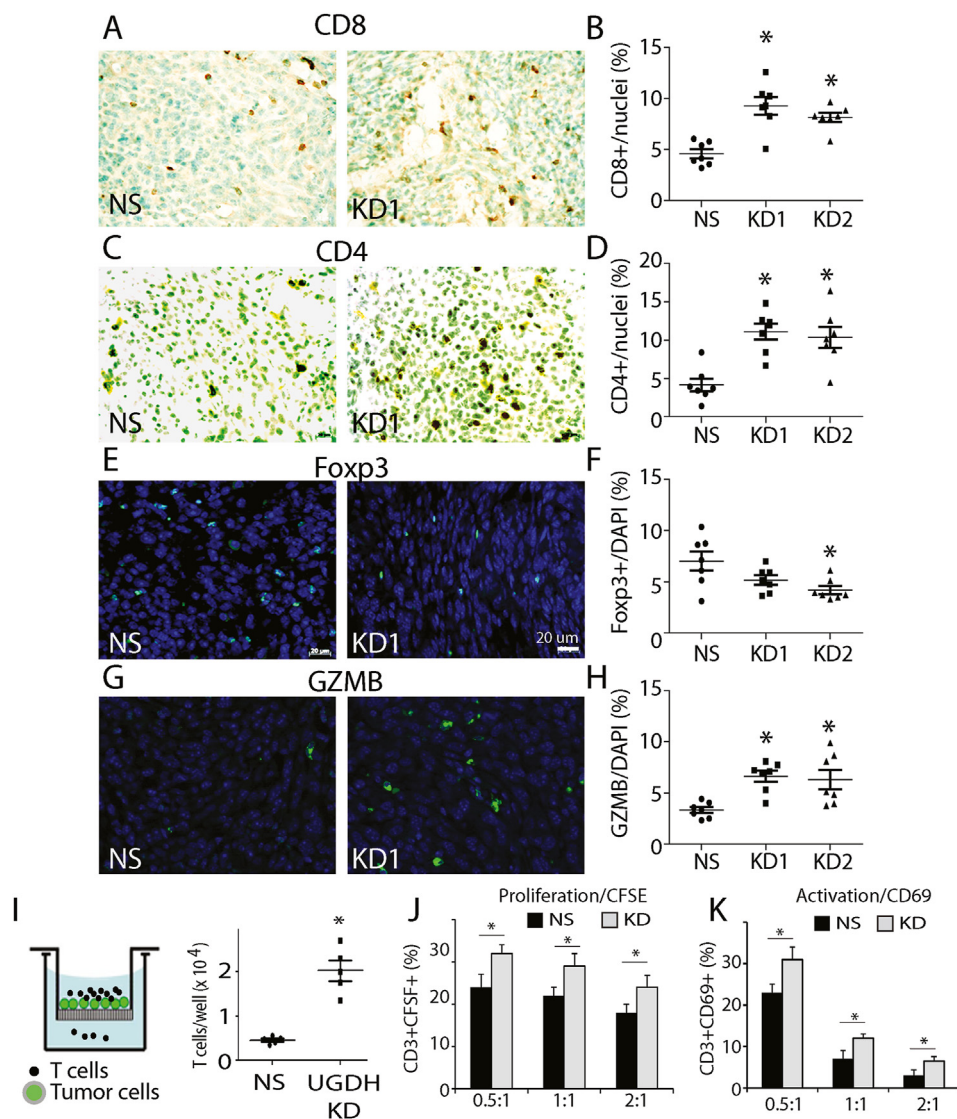
Figure 4 UGDH KD GBM cells promoted T cell infiltration and activation. **(A–D)** Immunohistochemistry (IHC) staining and quantification of CD4 and CD8 (dark brown) in control and UGDH KD GL261 tumors. Nuclei were counter-stained by methyl green. **(E–H)** IF staining and quantification of FoxP3 and granzyme B (GZMB) in mouse gliomas. **(I)** Human T cells were co-cultured with human GBM1A cells in transwells. UGDH KD GBM1A promoted T cell transmigration after 18 h in co-culture. **(J,K)** After co-culturing with control and UGDH KD GBM1A cells, flow cytometry analysis of human T cell proliferation based on CFSE signal (J) and activation based on CD69 signal (K). Data represent Mean ± SEM ($n = 5$). *: $P < 0.05$.

and GL261 cells (Fig. 5A) and potently inhibited GBM1A and GL261 cell growth and neurosphere formation (Fig. 5B–D, $P < 0.05$). To confirm the biological effect of 4-MU is dependent on ECM synthesis inhibition, we added exogenous high molecular weight HA (100 μg/ml) in GBM1A cells prior to 4-MU treatment. Exogenous HA significantly rescued the cells from growth inhibition by 4-MU (Fig. 5E, $P < 0.05$). ECM regulates cell adhesion and migration, and 4-MU treatment significantly decreased GBM1A cell migration in the transwell assay by ~60% (Fig. 5F, G). Similarly, the anti-migratory effect of 4-MU was reversed by exogenous HA (Fig. 5G, $P < 0.05$).

We examined the effect of 4-MU on macrophage phenotypes and GBM cell–macrophage interactions. 4-MU pretreatment in GBM cells (labeled with CFSE, FL1) increased macrophage phagocytosis capacity by ~50% (Fig. 5H, I). 4-MU itself did not affect macrophage polarization (data not shown). Adding 4-MU to GBM-macrophage co-cultures increased the expression of M1 polarization markers CD40/CD80/IL12B/TNFA (Fig. 5J, $P < 0.05$), consistent with our findings from macrophages co-cultured with UGDH KD GBM1A cells. However, 4-MU also increased the expression of M2 polarization markers CD163 and CD206 (Fig. 5J, $P < 0.05$). We further found that adding exogenous HA (high molecular weight, 100 μg/ml) in co-cultures prior to 4-MU treatment reversed macrophage gene expression induced by 4-MU (Fig. 5K, $P < 0.05$).
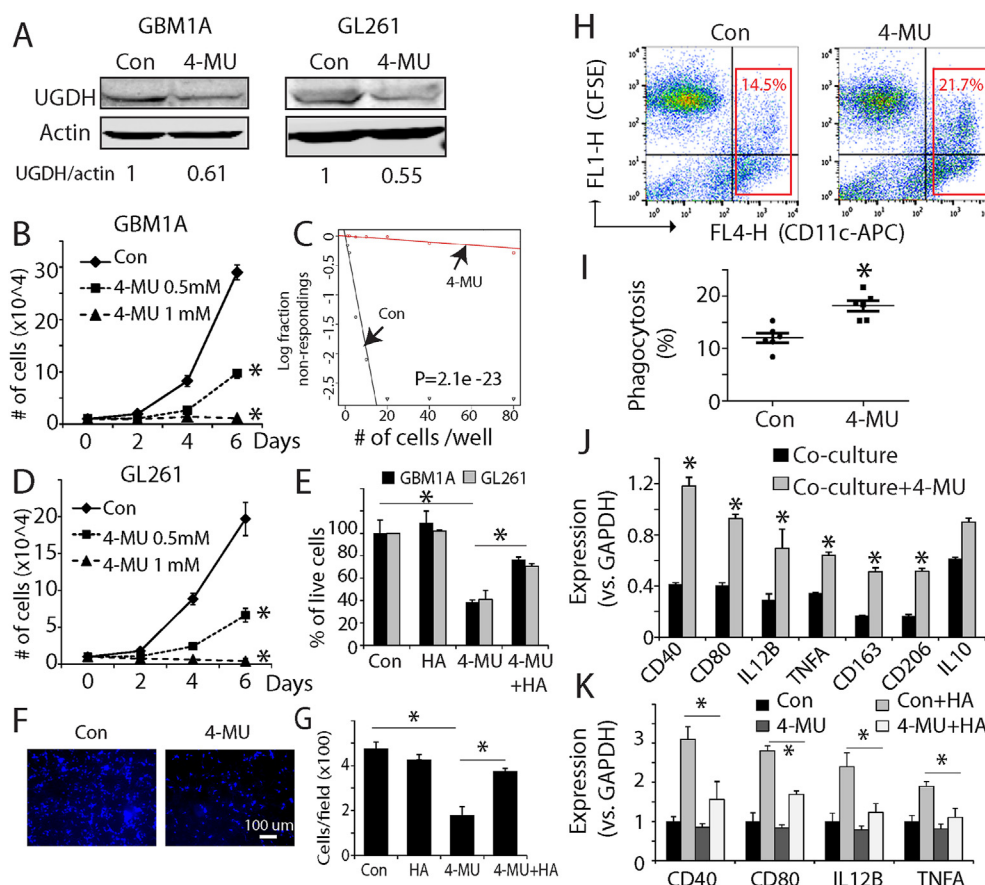
Figure 5   4-MU decreased GBM cell growth and activated macrophages *in vitro*. **(A)** Inhibition of UGDH expression by 4-MU (0.5 mM). **(B)** 4-MU decreased GBM1A proliferation in a dose-dependent manner. **(C)** Serial dilution assays showed 4-MU (0.5 mM, 14 days) decreased GBM1A neurosphere formation. **(D, E)** 4-MU (0.5 mM, 24 h) decreased GL261 proliferation, which was rescued by exogenous HA (100 μg/ml). **(F, G)** 4-MU inhibited GBM1A cell migration in transwell assays, and the anti-migratory effect of 4-MU was rescued by exogenous HA (100 μg/ml). **(H,I)** 4-MU pretreatment in GBM1A cells increased phagocytosis capacity of macrophages. **(J)** 4-MU increased the expression of M1 and M2 macrophage markers when added in the co-culture of human GBM1A cells and macrophages. **(K)** Exogenous HA reversed macrophage phenotype changes in co-cultures induced by 4-MU. Data represent Mean ± SEM ($n = 6$). *: $P < 0.05$.

4-MU inhibits glioma growth *in vivo*

4-MU has been shown to cross the brain-spinal cord barrier[16,28] predicting that it also crosses the blood–brain barrier. We established intracranial tumors from GL261 cells and tested if a previously established regimen of daily 4-MU (5% in mouse chow[31,32]) inhibited brain tumor growth. Animals were sacrificed 3 weeks after tumor cell implantation; brain sections were subjected to H&E and IF staining. 4-MU significantly decreased tumor growth with an average tumor size of 19 mm³ compared with 39 mm³ in the control-fed group (Fig. 6A, $P < 0.05$, $n = 8$ in total from two different independent experiments). We also examined the edge of tumors in the H& E stained sections. Both control and 4-MU treated tumors showed invasive phenotypes with irregular tumor edges, and there was no apparent difference between each other (Fig. 6B), indicating that 4-MU treatment did not influence tumor cell migration in the GL261 glioma model.

IF staining using a HA binding protein indicated that 4-MU dramatically decreased HA levels within the GL261 gliomas (Fig. 6C), consistent with CNS bioavailability and ECM

synthesis inhibition *in vivo*. Ki67 staining showed a significant decrease in tumor cell proliferation index after 4-MU treatment, with 26.5% Ki67 (*vs.* DAPI⁺) in control gliomas *vs.* 19.7% in 4-MU treated animals (Fig. 6D, $P < 0.05$).

4-MU treatment alters TAM polarization and increases glioma T cell infiltration *in vivo*

To examine the effect of 4-MU treatment on TAM phenotypes, we stained brain tumor sections for Iba-1 and CD107a. Iba1⁺ TAMs heavily infiltrated gliomas with no obvious difference in TAM morphology between control and 4-MU-treated groups. However, the density of Iba1⁺ TAMs (*vs.* DAPI⁺) significantly increased from 32% in control gliomas to 41% in 4-MU-treated tumors (Fig. 6E, F, $P < 0.05$). TAM expression of CD107a dramatically increased after 4-MU treatment, with a relative intensity of 145 (arbitrary number) in 4-MU-treated gliomas compared with 97 in control gliomas (Fig. 6E, F, $P < 0.05$). The association between tumor growth inhibition, increased TAM recruitment and TAM CD107a expression suggest that 4-MU induces TAMs
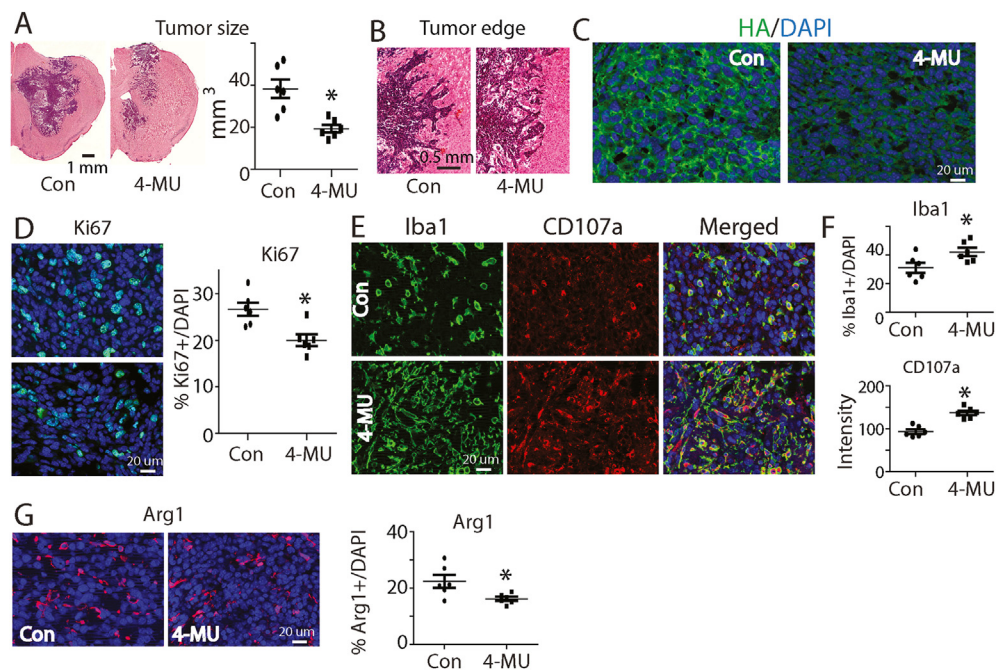
Figure 6 4-MU decreased mouse glioma growth *in vivo*. **(A)** H&E of mouse gliomas in control-fed and 4-MU-fed C57/BL mice. **(B)** Irregular tumor edges in control and 4-MU treated tumors. **(C)** IF staining of HA using a HA binding protein in tumor sections. **(D)** Ki67 staining showed a significant decrease in tumor cell proliferation after 4-MU treatment. **(E,F)** Iba1 and CD107a staining and quantification in control and 4-MU-treated gliomas. **(G)** IF staining of Arg1 in tumor sections. Data represent Mean $\pm$ SEM ($n = 6$). *: $P < 0.05$.

with anti-tumor activity. We also investigated the effect of 4-MU on expression of the M2 polarization marker Arg1 in the GL261 model. 4-MU decreased Arg-1$^+$ cells from ∼22% in controls to ∼17.5% (Fig. 6G, H, $P < 0.05$) without effecting the % of cells expressing the brain resident microglial marker TMEM119 (Fig. S5).

Furthermore, we examined the effect of 4-MU on T cell tumor infiltration and activation. 4-MU significantly increased CD8$^+$ T cell infiltration in tumors, with an average of 11.5% CD8$^+$ cells compared to 2.9% in the controls (Fig. 7A, B, $P < 0.05$); increased the % of CD4$^+$ cells from 5.9% to 17.3% (Fig. 7C, D, $P < 0.05$) and had no effect on Foxp3$^+$ cells (Fig. 7E, F). 4-MU increased infiltration of activated T cells as evidenced by ∼3 fold increase in the expression of GMZB$^+$ cells in 4-MU treated tumors (Fig. 7G, H, $P < 0.05$). These results show that 4-MU mimics effects of UGDH KD on glioma HA synthesis with similar biological effects including inhibition of tumor cell proliferation, promotion of phagocytic anti-tumor TAMs, and increased cytotoxic T cell infiltration and activation.

Discussion

The ECM is an important component of the brain tumor microenvironment. Since key components in the brain ECM, such as HA and tenascin C (TNC), heavily participate in the innate and adaptive immune response, our current work investigates how targeting ECM synthesis impacts tumor cell−immune cell interactions. For the first time, we found that targeting UGDH in GBM cells, the critical enzyme of

GAG synthesis, promoted the anti-tumor function and phagocytic activation of TAMs and increased cytotoxic T cell infiltration and activation *in vivo*. Moreover, we demonstrated that pharmacologically targeting ECM synthesis with 4-MU inhibited glioma growth by directly reducing tumor cell proliferation and promoting the anti-tumor function of TAMs and T cells. This work advances our understanding of the biological impact of UGDH and suggests that targeting ECM synthesis alone or in combination with other anti-tumor strategies is promising to inhibit GBM growth. Notably, no isoenzyme shares a similar function as UGDH,[11] greatly reducing the concern of compensatory effects when targeting UGDH in preclinical models and ultimately in patients.

Numerous studies have shown HA and many other GAGs, the end product of UGDH, are involved in solid tumor growth and tumor immune responses.[33,34] For example, HA binds to its cognate receptor CD44, commonly expressed in immune cells (macrophages and T cells), thereby activating downstream signaling pathways (i.e., AKT, MAPK) and influencing immune response. The therapeutic potential of ECM synthesis inhibition is further substantiated by numerous efforts focusing on targeting HA synthesis to treat solid tumors.[35,36] The effect of HA on the innate and adaptive immune systems has been mainly reported in many inflammatory and autoimmune diseases such as encephalomyelitis (EAE).[28] However, the effect of UGDH in the brain tumor immune microenvironment has not been fully understood. In our previous study,[13] we focused on the impact of targeting UGDH on ECM synthesis and tumor cell proliferation/migration. Here, we further extended our
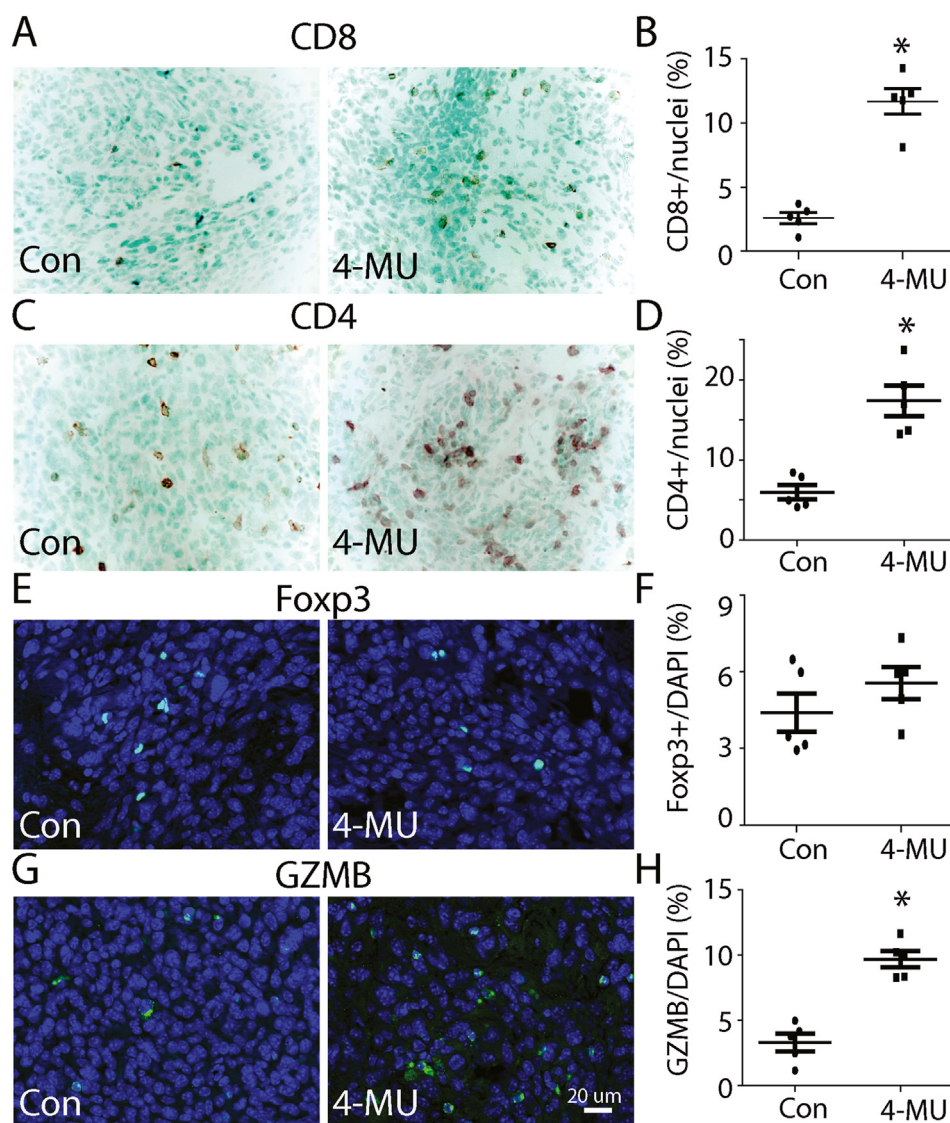
Figure 7 4-MU treatment promoted T cell infiltration and activation in mouse gliomas. **(A—D)** Immunohistochemistry (IHC) staining and quantification of CD4 and CD8 (dark brown) in control and 4-MU-treated GL261 tumors. Nuclei were counter-stained by methyl green. **(E—H)** IF staining and quantification of FoxP3 and (GZMB) in control and 4-MU treated mouse gliomas. Data represent Mean $\pm$ SEM ($n = 5$). *: $P < 0.05$.

findings in mouse glioma models. Compared with human glioma cells, even though UGDH knockdown did not significantly affect GL261 mouse glioma cell growth *in vitro* and *in vivo*, we still found that tumors from UGDH knockdown GL261 cells grow much slower than those from control cells. This suggests that UGDH knockdown influences the TME to decrease tumor growth.

Indeed, our current study further revealed multiple functions of UGDH in brain tumor malignancy. We demonstrated that UGDH knockdown and 4-MU treatment significantly decreased ECM components, especially HA abundance in the tumor microenvironment. Therefore, the decreased expression of HA subsequently impacts the phenotypes and behavior of adjacent immune cells, possibly through the interaction with its receptors. One of the main findings is

that genetically or pharmacologically targeting ECM synthesis promoted the phagocytic activity of TAMs to contribute to tumor suppression. TAMs consist of 30—40% of a tumor mass and are predominantly associated with pro-tumor and anti-inflammatory functions to promote tumor growth. However, TAMs are heterogeneous with high plasticity; if properly activated, TAMs can elicit anti-tumor functions. In our study, we realized some discrepancy in macrophage phenotype changes in co-culture systems (M1-like polarization) and *in vivo* experiments (decreased M2-like TAMs), this may stem from various phenotypes of immune cells under different conditions. We think both results are important: despite these differences, both scenarios indicate that decreased GAG synthesis in tumor cells resulted in an immune stimulating tumor microenvironment.

In our model, we found targeting UGDH stimulated the phagocytic activity of TAMs in SCID mice, as evidenced by the increase in lysosome marker CD107. Although SCID mice did not have an effective adaptive immune system, they still have an intact innate immune system. Our findings of the cross-species tumor cell—TAM interactions in SCID mice were further confirmed in human GBM cell—macrophage co-cultures and in syngeneic mouse glioma models that contain an immunocompetent immune system. We also examined the expression of M1 and M2 polarization markers in TAMs *in vivo* and found no induction of M1 polarization of TAMs associated with the anti-tumor function of TAMs. Based on our studies, we propose that the anti-tumor role of TAMs is mainly associated with an increased phagocytic capacity of TAMs instead of inducing an M1 pro-inflammatory state.

Among decades of research showing the importance of the ECM in tumor malignancy, the influence of ECM on T cell functions has been recognized in solid tumors. Studies have shown that sufficient T cell infiltration in tumor tissues is a prerequisite for the response to PD-1/PD-L1 blockade.[37] The ECM plays a critical role in inhibiting cytotoxic T cell function.[38] For example, tenascin C has been reported to inhibit T cell activation[39,40]; dense ECM prevents T cell access to tumor cells.[8] Thus, targeting the ECM is expected to have a significant impact on tumor T cell interactions. Our studies indicated that targeting UGDH in GBM cells promotes T cell infiltration and activation in brain tumors in syngeneic mouse models. In human glioma, T cell-based immune checkpoint inhibition has not proven to be effective in inhibiting tumor growth; one of the reasons may be sparse T cells in gliomas. It has been reported that T cells consist of less than 1% of a tumor mass.[41] Our current work is consistent with the role of the ECM in T cell function and suggests that targeting UGDH reverses tumor immune evasion and turns a "cold" tumor (lack of T cell infiltration) into "hot". In the future, we will test if targeting UGDH can be combined with immune checkpoint blockade to prevent tumor growth.

Currently, only a few small molecules have been reported to inhibit UGDH function. Besides 4-MU, quercerin and galic have been reported to inhibit UGDH enzymatic functions.[14] We found 4-MU potently inhibits GBM cell proliferation. 4-MU mimics the effect of UGDH knockdown by depleting the ECM precursor UDP-GlcUA[15] and down-regulating UGDH[15] and hyaluronan synthases.[16] Recently, Pibuel et al[42] reported the anti-GBM function of 4-MU in GL26 cells *in vitro*. We demonstrated that in mouse syngeneic glioma models, daily 4-MU treatment significantly decreased glioma cell growth *in vivo*, suggesting that 4-MU could cross the blood—brain barrier to inhibit ECM synthesis and GBM growth. The tumor inhibition effect of 4-MU is probably a combination of reduced tumor cell proliferation and increased anti-tumor function of TAMs in moue brains, consistent with our findings in UGDH KD tumor models in SCID and syngeneic mice. 4-MU treatment also increased cytotoxic T cell infiltration and activation in GL261 UGDH gliomas, suggesting that inhibiting ECM synthesis by 4-MU can be combined with T cell-based immune checkpoint blockade to treat GBM.

Reasons for GBM treatment failure include but are not limited to uncontrolled tumor cell proliferation/migration,

cancer stem cells, GBM cell heterogeneity, immune evasion, and the BBB. Inhibiting ECM synthesis can overcome many obstacles for effective GBM treatment by simultaneously targeting tumor cells and the TME, potentially leading to improved therapeutic outcomes. Our studies determine the biological function of UGDH in brain tumors and suggest that UGDH is not only essential for GBM cell proliferation/migration but also vital for tumor immune evasion. Understanding the effect of ECM synthesis inhibition on the interactions between GBM cells and immune cells will guide the development of effective combinatory anti-cancer therapies, such as anti-CD47 antibodies and immune checkpoint blockade. Given the widespread importance of the ECM in other malignancies, positive results generated from our models can be extrapolated to other solid tumors.

Author contributions

D. Z., F. Y. and D. M.: conducted experiments, data collection, figure preparation, and manuscript writing; Y. F., S. W., B. L. and Y. L.: conducted experiments and data collection; O. D., M. Y., and J. L.: financial support and manuscript writing; H. L. and S.X.: experiment design, financial support, figure preparation, and manuscript writing.

Conflict of interests

The authors indicate no potential conflicts of interest.

Funding

Appendix A. Supplementary data

Supplementary data to this article can be found online at https://doi.org/10.1016/j.gendis.2021.08.008.

References

1. Cloughesy TF, Cavenee WK, Mischel PS. Glioblastoma: from molecular pathology to targeted treatment. *Annu Rev Pathol*. 2014;9:1—25.
2. Lim M, Xia Y, Bettegowda C, Weller M. Current state of immunotherapy for glioblastoma. *Nat Rev Clin Oncol*. 2018; 15(7):422—442.
3. Hambardzumyan D, Gutmann DH, Kettenmann H. The role of microglia and macrophages in glioma maintenance and progression. *Nat Neurosci*. 2016;19(1):20—27.
4. Lu P, Weaver VM, Werb Z. The extracellular matrix: a dynamic niche in cancer progression. *J Cell Biol*. 2012;196(4):395—406.
5. Brown Y, Hua S, Tanwar PS. Extracellular matrix-mediated regulation of cancer stem cells and chemoresistance. *Int J Biochem Cell Biol*. 2019;109:90—104.
6. Yue B. Biology of the extracellular matrix: an overview. *J Glaucoma*. 2014;23(8 Suppl 1):S20—S23.

7. Wolf K, Te Lindert M, Krause M, et al. Physical limits of cell migration: control by ECM space and nuclear deformation and tuning by proteolysis and traction force. *J Cell Biol*. 2013; 201(7):1069—1084.

8. Salmon H, Donnadieu E. Within tumors, interactions between T cells and tumor cells are impeded by the extracellular matrix. *Oncoimmunology*. 2012;1(6):992—994.

9. Song I, Dityatev A. Crosstalk between glia, extracellular matrix and neurons. *Brain Res Bull*. 2018;136:101—108.

10. Chen J, Yang S. Catalytic mechanism of UDP-glucose dehydrogenase. *Biochem Soc Trans*. 2019;47(3):945—955.

11. Egger S, Chaikuad A, Kavanagh KL, Oppermann U, Nidetzky B. UDP-glucose dehydrogenase: structure and function of a potential drug target. *Biochem Soc Trans*. 2010;38(5):1378—1385.

12. Spicer AP, Kaback LA, Smith TJ, Seldin MF. Molecular cloning and characterization of the human and mouse UDP-glucose dehydrogenase genes. *J Biol Chem*. 1998;273(39):25117—25124.

13. Oyinlade O, Wei S, Lal B, et al. Targeting UDP-α-D-glucose 6-dehydrogenase inhibits glioblastoma growth and migration. *Oncogene*. 2018;37(20):2615—2629.

14. Hwang EY, Huh JW, Choi MM, Choi SY, Hong HN, Cho SW. Inhibitory effects of gallic acid and quercetin on UDP-glucose dehydrogenase activity. *FEBS Lett*. 2008;582(27):3793—3797.

15. Clarkin CE, Allen S, Wheeler-Jones CP, Bastow ER, Pitsillides AA. Reduced chondrogenic matrix accumulation by 4-methylumbelliferone reveals the potential for selective targeting of UDP-glucose dehydrogenase. *Matrix Biol*. 2011;30(3):163—168.

16. Mueller AM, Yoon BH, Sadiq SA. Inhibition of hyaluronan synthesis protects against central nervous system (CNS) autoimmunity and increases CXCL12 expression in the inflamed CNS. *J Biol Chem*. 2014;289(33):22888—22899.

17. Nagy N, Kuipers HF, Frymoyer AR, et al. 4-methylumbelliferone treatment and hyaluronan inhibition as a therapeutic strategy in inflammation, autoimmunity, and cancer. *Front Immunol*. 2015;6:123.

18. Galli R, Binda E, Orfanelli U, et al. Isolation and characterization of tumorigenic, stem-like neural precursors from human glioblastoma. *Cancer Res*. 2004;64(19):7011—7021.

19. Li Y, Li A, Glas M, et al. c-Met signaling induces a reprogramming network and supports the glioblastoma stem-like phenotype. *Proc Natl Acad Sci U S A*. 2011;108(24): 9951—9956.

20. Hu Y, Smyth GK. ELDA: extreme limiting dilution analysis for comparing depleted and enriched populations in stem cell and other assays. *J Immunol Methods*. 2009;347(1—2): 70—78.

21. Wang SD, Rath P, Lal B, et al. EphB2 receptor controls proliferation/migration dichotomy of glioblastoma by interacting with focal adhesion kinase. *Oncogene*. 2012;31(50):5132—5143.

22. Jin X, Kruth HS. Culture of macrophage colony-stimulating factor differentiated human monocyte-derived macrophages. *J Vis Exp*. 2016;112:54244.

23. Cho HJ, Shashkin P, Gleissner CA, et al. Induction of dendritic cell-like phenotype in macrophages during foam cell formation. *Physiol Genomics*. 2007;29(2):149—160.

24. Ma D, Liu S, Lal B, et al. Extracellular matrix protein tenascin C increases phagocytosis mediated by CD47 loss of function in glioblastoma. *Cancer Res*. 2019;79(10):2697—2708.

25. Xia S, Rosen EM, Laterra J. Sensitization of glioma cells to Fas-dependent apoptosis by chemotherapy-induced oxidative stress. *Cancer Res*. 2005;65(12):5248—5255.

26. Lal B, Goodwin CR, Sang Y, et al. EGFRvIII and c-Met pathway inhibitors synergize against PTEN-null/EGFRvIII+ glioblastoma xenografts. *Mol Cancer Ther*. 2009;8(7):1751—1760.

27. Kuipers HF, Nagy N, Ruppert SM, et al. The pharmacokinetics and dosing of oral 4-methylumbelliferone for inhibition of hyaluronan synthesis in mice. *Clin Exp Immunol*. 2016;185(3):372—381.

28. Kuipers HF, Rieck M, Gurevich I, et al. Hyaluronan synthesis is necessary for autoreactive T-cell trafficking, activation, and Th1 polarization. *Proc Natl Acad Sci U S A*. 2016;113(5): 1339—1344.

29. Huynh KK, Eskelinen EL, Scott CC, Malevanets A, Saftig P, Grinstein S. LAMP proteins are required for fusion of lysosomes with phagosomes. *EMBO J*. 2007;26(2):313—324.

30. Jeng MY, Hull PA, Fei M, et al. Metabolic reprogramming of human CD8+ memory T cells through loss of SIRT1. *J Exp Med*. 2018;215(1):51—62.

31. Tamura R, Yokoyama Y, Yoshida H, Imaizumi T, Mizunuma H. 4-Methylumbelliferone inhibits ovarian cancer growth by suppressing thymidine phosphorylase expression. *J Ovarian Res*. 2014;7:94.

32. Yates TJ, Lopez LE, Lokeshwar SD, et al. Dietary supplement 4-methylumbelliferone: an effective chemopreventive and therapeutic agent for prostate cancer. *J Natl Cancer Inst*. 2015;107(7):djv085.

33. Anderson KG, Stromnes IM, Greenberg PD. Obstacles posed by the tumor microenvironment to T cell activity: a case for synergistic therapies. *Cancer Cell*. 2017;31(3):311—325.

34. Di Modugno F, Colosi C, Trono P, Antonacci G, Ruocco G, Nisticò P. 3D models in the new era of immune oncology: focus on T cells, CAF and ECM. *J Exp Clin Cancer Res*. 2019; 38(1):117.

35. Karousou E, Misra S, Ghatak S, et al. Roles and targeting of the HAS/hyaluronan/CD44 molecular system in cancer. *Matrix Biol*. 2017;59:3—22.

36. Vitale D, Kumar Katakam S, Greve B, et al. Proteoglycans and glycosaminoglycans as regulators of cancer stem cell function and therapeutic resistance. *FEBS J*. 2019;286(15):2870—2882.

37. Tang H, Wang Y, Chlewicki LK, et al. Facilitating T cell infiltration in tumor microenvironment overcomes resistance to PD-L1 blockade. *Cancer Cell*. 2016;29(3):285—296.

38. Dustin ML, de Fougerolles AR. Reprogramming T cells: the role of extracellular matrix in coordination of T cell activation and migration. *Curr Opin Immunol*. 2001;13(3):286—290.

39. Hemesath TJ, Marton LS, Stefansson K. Inhibition of T cell activation by the extracellular matrix protein tenascin. *J Immunol*. 1994;152(11):5199—5207.

40. Hibino S, Kato K, Kudoh S, Yagita H, Okumura K. Tenascin suppresses CD3-mediated T cell activation. *Biochem Biophys Res Commun*. 1998;250(1):119—124.

41. Han S, Ma E, Wang X, et al. Rescuing defective tumor-infiltrating T-cell proliferation in glioblastoma patients. *Oncol Lett*. 2016;12(4):2924—2929.

42. Pibuel MA, Diaz M, Molinari Y, et al. 4-Methylumbelliferone as a potent and selective antitumor drug on a glioblastoma model. *Glycobiology*. 2021;31(1):29—43.